Soft Matter

Modeling gas transport in polymer-grafted nanoparticle membranes

SCHOLARONE™
Manuscripts

Soft Matter

Modeling gas transport in polymer-grafted nanoparticle membranes[†]

J. Wesley Barnett and Sanat K. Kumar[‡]

We use coarse-grained Molecular Dynamics simulations to study gas diffusion within nanocomposites consisting of matrix-free polymer-grafted nanoparticles. We compare the transport of gas penetrants in systems using polymer models with and without an angle potential and show that gas diffusion enhancement occurs in nanocomposite systems only with the angle potential. This enhancement is related to the free volume in the system, but the cage size experienced by the gas penetrant seems to be a more relevant indicator of gas diffusion enhancement. The enhancement seen in our simulations is smaller than that observed in experiments.

1 Introduction

Polymeric membranes are an economically-attractive way to separate gases in industrial processes and have been used for over 40 years in commercial settings.[1–3] Such membranes are used in the separation of oxygen from air, hydrogen recovery, and the removal of CO2 from CO2/natural gas mixtures. Polymer membranes are also an option for carbon capture.[4–7]

Gas transport across polymeric membranes that obey the solution-diffusion model[8] is described using the following relationship:

$$J = \frac{P \Delta p}{\ell} \qquad (1)$$

In this equation J is the flux across the membrane, P is the permeability, Δp is the pressure drop across the membrane, and ℓ is the membrane thickness. P is a material property specific to each polymeric membrane. When two gases diffuse across the membrane in a separation process, the ideal selectivity is defined as:

$$\alpha_{A/B} = \frac{P_A}{P_B} \qquad (2)$$

In this equation P_A is the permeability of gas A across the membrane, and P_B is the permeability of gas B. Thus, the performance of a polymeric membrane in separating a binary mixture of gases can be described using both its permeability and selectivity.

By plotting the permeability and selectivity of gas pairs for a variety of polymers, it is observed that there is an upper limit—known as the "Robeson upper bound".[9,10] This upper bound indicates an intrinsic trade-off between selectivity and permeability. Polymers near the upper bound generally tend to be glassy, and thus exhibit a sieving mechanism based on the ratio of the gas particle sizes.[11]

Significant effort has been devoted to improving the performance of gas separation membranes.[12–18] One possible pathway to enhancing permeabilities in polymer membranes is the use of polymer nanocomposites, specifically combining polymers with inorganic nanofillers ("mixed matrix membranes"). One advantage to nanofillers is that the mechanical properties of the polymer membrane can be enhanced by their addition.[19] Additionally, in some cases, nanofillers help to slow membrane aging.[20]

Historically, however, the addition of fillers in many cases suppresses gas permeability.[21] Most often this permeability suppression is described using the Maxwell relationship,[22,23] where ϕ is the volume fraction of filler material, P_ϕ is the permeability within the nanocomposite, and P_b is the permeability within the neat polymer:

$$\frac{P_\phi}{P_b} = \left(\frac{1-\phi}{1+\frac{\phi}{2}} \right) \qquad (3)$$

In this expression the ratio P_ϕ/P_b is always less than 1.

Gas permeability within polymer membranes has been shown to be correlated with free volume[25,26]—an empirically defined quantity thought to describe the unoccupied spaces between polymer segments, reflecting the local motion of the chain segments[27]—and in contrast to above, in some instances it has been shown that the addition of nanoparticles can enhance gas permeability by increasing the free volume of the polymer phase.[28,29] Maintaining particle dispersion is of key importance in achieving gas permeability enhancements,[30] and the use of polymer-grafted nanoparticles can prevent aggregation, especially in a matrix-free system.[31] Recent experimental work has shown that poly(methyl

Department of Chemical Engineering, Columbia University, New York, NY 10027, United States

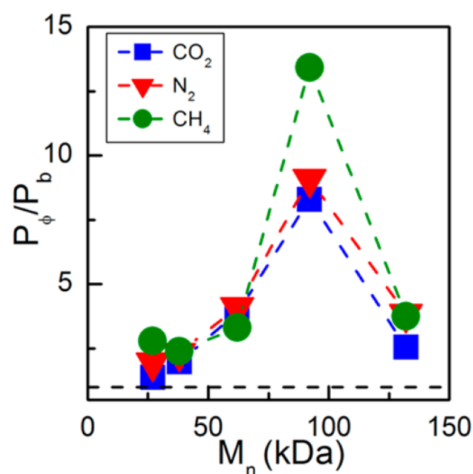‡ To whom correspondence should be addressed. Email: sk2794@columbia.edu.

Fig. 1 Relative gas permeabilities of gases in composite systems relative to that of neat poly(methyl acrylate) (PMA). Composite systems consisted of spherical silica nanoparticles grafted with PMA. Neat PMA is presented as the dashed line at $P_\phi/P_b = 1$. Reprinted (adapted) with permission from Reference 24. Copyright 2017 American Chemical Society.

acrylate) (PMA) grafted and poly(methyl methacrylate) (PMMA) grafted silica nanoparticles in a matrix-free system can maintain particle dispersion and enhance gas permeability relative to that in the corresponding neat polymer systems. In some cases, gas permeabilities in the composite material are 8-13 times that of permeabilities in the corresponding neat melt, depending on the grafted polymer length (Figure 1).[24]

Computer simulations allow for the investigation of polymer nanocomposites and the factors that lead to gas permeability enhancement. The permeability of a gas in a polymer or polymer nanocomposite membrane can be decomposed into the diffusivity (D) and solubility (S) according to the following relationship:[8,32]

$$P = DS \tag{4}$$

For materials near the glass-transition temperature variations in the diffusivity dominates this equation and changes in the solubility can be neglected. The diffusion coefficient of gas particles can be calculated in computer simulations through its relationship to the mean-squared displacement (Equation 8).

Coarse-grained computer simulations have shown that it is necessary to carefully select the gas penetrant size and the polymer temperature—or, equivalently, density—in order to model gas diffusion in separation membranes. That is, gas diffusion is—empirically—an activated process, and coarse-grained simulations must be set up with the appropriate parameters to capture this. Zhang, *et. al.*[33], systematically varied the gas particle size and system temperature and showed that the diffusion coefficient of gas penetrants falls into three possible regimes, related to the size of the particle and temperature; only one of these regimes models the activated diffusion process relevant to experimental gas separation processes. They showed that transport of gas particles with diameter d smaller than a critical diameter d_c is in a kinetic regime where $D \sim Te^{-kd}$. For gas particles that are of the same size or larger than the monomer segment size (σ), diffusion

is in a power law regime ($D \sim Td^{-n}/g(T)$).

Gas transport is only in the activated regime ($D \sim Te^{-E_a(d)/k_BT}$) for particles with $d_c < d < \sigma$. Additionally they showed that the monomer number density (ρ) needs to be larger than a minimum density (ρ_c) for gas transport to be in the activated regime and not the kinetic regime. For their "flexible" model $\rho_c = 0.9$ and $d_c = 0.25\sigma$ and for their rigid model (with an added angle potential) $\rho_c = 1.12$ and $d_c = 0.4\sigma$ for gas particle transport to be in the activated regime.

Zhang, *et. al.*'s work focused solely on transport in neat melts, but coarse-grained simulations have also been used to investigate gas transport in nanocomposites. Gansesan has demonstrated gas diffusion enhancement in nanocomposites using coarse-grained kinetic Monte Carlo simulations.[34] Those simulations used the bond-fluctuation model where dynamic asymmetry was enforced by artificially slowing the chain motion relative to that of the gas motion. He showed that gas diffusion can be enhanced to 8-10 times of that in a neat melt with the addition of bare particles to free glassy chains. In that work, gas penetrants were modeled to be the same size as the polymer segments, and thus gas diffusion is in the power law regime. Additionally, the systems were modeled in the canonical ensemble (constant N, V, and T) and nanoparticles were made immobile. Ganesan showed that as chain rigidity increased, gas penetrant diffusion in the nanocomposite became more enhanced relative to that in the neat, which inspired us to investigate polymer models both with and without rigid angle potentials.

In this work we use coarse-grained Molecular Dynamics simulations to study the diffusion of gas penetrants within neat polymer systems and nanocomposites consisting of polymer-grafted nanoparticles. In contrast to Ganesan's work, we model our systems in the isothermal-isobaric ensemble (constant N, P, and T) and allow nanoparticles to move, with particle mobilities naturally arising from the interactions between particles. We use the same flexible and rigid models in Zhang, *et. al.*'s study[33] and vary the system pressure in order to meet the minimum densities required for activated diffusion (see Methods). Additionally we select $d_c < d < \sigma$ for our systems so that they are always in the activated diffusion regime. Our model does show enhancement in gas diffusion in nanocomposites of about 1.3 times that in the neat melt, still well below experimental observations. We show how D is related to the fractional free volume in the polymer phase and propose an explanation on why our model does not capture the magnitude and chain-length dependence of previous experimental observations.

2 Methods

Molecular Dynamics simulations were performed using LAMMPS.[35] All simulations were performed in the isothermal-isobaric ensemble.[36–39] The Lennard-Jones 6-12 potential was used to model interactions with ε set to 1.0 for nanoparticles, polymer segments, and gas particles, and thus for all interactions. The mass (m_0) was set to 1.0 for polymer segments, 1.0 for gas particles, and 125.0 for nanoparticles. (Our previous results show that the mass of the gas particles do not qualitatively affect the results obtained.) Polymer segment diameters were defined

to be σ. Gas penetrant diameters were defined to be 0.5σ. Nanoparticles were modeled using an expanded Lennard-Jones potential:

$$E_{ij} = 4\varepsilon\left[\left(\frac{\sigma_{ij}}{r_{ij}-\Delta_{ij}}\right)^{12} - \left(\frac{\sigma_{ij}}{r_{ij}-\Delta_{ij}}\right)^{6}\right] \qquad r < r_c + \Delta_{ij} \quad (5)$$

Δ_{ij} was set to $(5\sigma_i + \sigma_j)/2.0 - 1.0$ so that nanoparticle diameter was set to 5σ, where particle i is the nanoparticle with $\sigma_i = \sigma$ and particle j is a polymer segment, a gas particle, or another nanoparticle. All interactions were shifted and cut off at $r_c = 1.12\sigma_{ij}$ such that only repulsions were included in interactions, where σ_{ij} was defined according to the Lorentz rule, $\sigma_{ij} = (\sigma_i + \sigma_j)/2$.
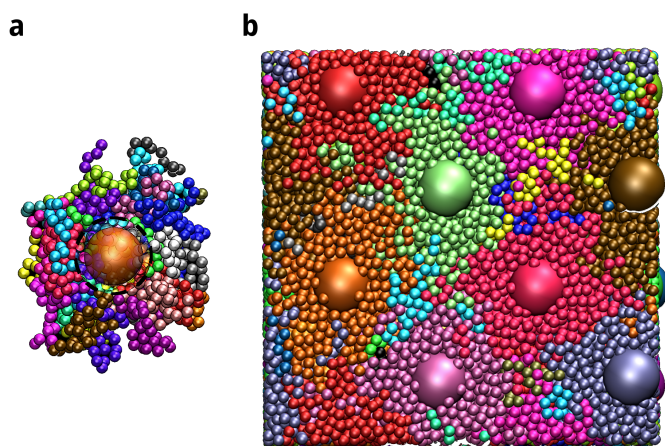
a　　　　**b**

Fig. 2 Snapshots of system simulated at P* = 20 for the rigid model. **a** Snapshot of a single grafted nanoparticle with the surrounding nanoparticles removed for clarity. Different colors represent individual grafted chains. The area within the dashed black circle is semi-transparent in order to see the particle. **b** System of nanoparticles cut by a plane. Different colors represent nanoparticles and their associated grafted chains.

The bonds connecting beads in chains were modeled using the finite extensible elastic potential:

$$U_{FENE}(r) = -0.5KR_0^2 \ln\left[1 - (r/R_0)^2\right] \qquad r < R_0 \quad (6)$$

K was set equal to $30\varepsilon/\sigma^2$ and R_0 set to 1.5σ, where ε is the unit of energy.[40]

Neat systems contained 250 polymers each with 40 segments. Nanocomposite systems contained 32 nanoparticles, each with 30 chains grafted to them, also with 40 segments each. Chains were grafted to fixed points on the nanoparticle. Each system contained 100 gas penetrants—thus, we model the tracer limit. Nanoparticles were arranged in a dilute FCC lattice (no overlaps) before pressure was turned on immediately to the specified setting below. Particles were allowed to move freely. We do not know if the final NP structure is a consequence of the initial FCC lattice on which they were arranged, and hence we do not know the effect of this starting state on the results reported.

Two models were simulated for both the neat and composite systems:

1. **Model I (flexible).** In this model no additional angle poten-

tial was used for the polymers.

2. **Model II (rigid angles).** This model is identical to Model I with the exception that a harmonic angle potential was added for polymers with the following functional form:

$$U_\theta = K_\theta(\theta - \theta_0)^2 \quad (7)$$

K_θ was set equal to 300ε rad^{-2} and θ_0 to $109.5°$. These values were picked to follow Zhang, et. al.'s model.[33,41]

It is well known that the Kremer-Grest bead spring model is extremely coarse grained. Thus, there is no unequivocal means of assigning what a bead really means. Extensive work shows that the fully flexible model has a persistence length of 1.3 monomer diameters. Thus, the monomer diameter is not the Kuhn length, but something close. The addition of a bond bending potential causes stiffness to go up; this has been discussed extensively in our previous work and that of Grest. However, the chains do not become liquid-crystalline since there are no torsional constraints.

Flexible systems were simulated at P* = 5, 10, 15, 20, 24, 28, 32, 36 (P* = Pσ^3/ε). Rigid systems were simulated at P* = 5, 10, 15, 20, 24, and 28. Each system was simulated with the reduced temperature set to 1.0 (T* = k_BT$/\varepsilon$). A reduced timestep of $\Delta\tau = 0.012$ ($\tau = t\sqrt{\varepsilon/m_0}/\sigma$) was used for the flexible systems, and a reduced timestep of $\Delta\tau = 0.006$ was used for the rigid systems.

After pressure was turned on for each system, bond swapping was attempted every 5 steps for $1.2\times10^5\tau$ in order to speed up equilibration.[42] From there, each system was equilibrated additionally between $1.2\times10^5\tau$ and $2.5\times10^6\tau$ until the volume of the system equilibrated. Production runs were performed for $1.08\times10^6\tau$.

We additionally performed a series of simulations of Model II composite systems with a varying number of segments on each grafted chain, simulating systems with 5 segments per chain up to 70 segments per chain, at 5-segment increments. These systems were simulated at P* = 20. Bond swapping was not performed for these systems, since for this model bond swapping only occurred $\sim 0.0001\%$ of the time, compared to $\sim 1\%$ for Model I.

Diffusion coefficients of gas penetrants were calculated using the mean-squared displacement of the gas penetrants (Einstein relationship), using the MSD values from the last $1.2\times10^4\tau$ of each simulation, ensuring that the gas has reached the diffusion regime (Figures S5 and S6):

$$D = \langle(r(t) - r(0))^2\rangle/6t \quad (8)$$

Given that we have performed only one long simulation in each case, we first verify that a plot of $\frac{\langle(r(t)-r(0))^2\rangle}{t}$ assumes a time-independent plateau. An error estimate then corresponds to the uncertainty in this long-time plateau. We find typical estimates to be less than 20% in all cases, which therefore represents a conservative error bar for the diffusivity data.

The "partial" molar volume of adding a nanoparticle to a neat system and then grafting it was calculated as follows:

$$\Delta V = \frac{V_{comp} - V_{neat}}{N_{np}} \quad (9)$$

V_{comp} is the volume of the composite system, V_{neat} is the volume of

the neat system scaled to the same number of polymer segments as the composite system, and N_{np} is the number of nanoparticles in the composite system.

The polymer phase segment number density (ρ_{poly}) was determined by first calculating the segment–segment radial density function for the nanocomposite systems (Figures S1-S4). The density at large distances is the bulk polymer density (ρ_{bulk}). This bulk density includes volume occupied by the nanoparticles for the nanocomposite system which needs to be removed since we are only interested in the polymer phase density:

$$\rho_{poly} = \rho_{bulk} \frac{V}{V_{poly}} = \rho_{bulk} \frac{V}{V - V_{np}} \tag{10}$$

Here V is the average volume of the entire system, V_{poly} is the volume of the polymer phase, and V_{np} is the total volume of all nanoparticles in the system determined as:

$$V_{np} = N_{np} \frac{4}{3} \pi \left(\left(\frac{5\sigma}{2} \right)^3 + \frac{30}{2} \left(\frac{\sigma}{2} \right)^3 \right) \tag{11}$$

The first term is the hard core volume of a nanoparticle itself, which we use since only repulsions are present in the simulation and any error introduced into the volume would be minimal because only 32 particles are present. The second term comes from the thirty points on each nanoparticle's surface where polymer chains are grafted which are approximately one-half the volume of a polymer segment. The graft points are in this calculation since they are not present in the neat melt.

The fractional free volume of the polymer phase was defined as follows using the volume occupied by polymer chains ($V_{o,poly}$) and the polymer phase volume (V_{poly}):[43]

$$FFV = 1 - \frac{V_{o,poly}}{V_{poly}} = 1 - \frac{V_{vdw,total} - V_{np}}{V - V_{np}} \tag{12}$$

where $V_{vdw,total}$ is the summation of the van der Waals volumes of all particles in the system, V_{np} is defined in Equation 11, and V is the average volume of the entire system. Typically $V_{o,poly}$ is set equal to the summation of the van der Waals volume of all polymer segments multiplied by some prefactor. Here we set the prefactor to 1 and therefore $V_{o,poly}$ equals the summation of the van der Waals volume of all polymer segments.

3 Results and Discussion

3.1 Polymer segment mean-squared displacements

The mean-squared displacements (MSD) of polymer segments (Figure 3) show that for the lowest reduced pressures studied the neat systems transition from the ballistic regime to the diffusive regime (MSD $\sim \tau$). The neat flexible systems with P* $\leq$ 15 and the neat rigid system with P* = 5 are diffusive by $10^6\tau$. Since some systems are not diffusive on the time scale of the simulations, we cannot guarantee that the systems are fully equilibrated. This is the case especially for P* $\geq$ 20 for flexible systems, and P* $\geq$ 10 for rigid systems.

The MSDs of the flexible systems show that the polymers become glassier as P* increases with the sub-diffusive region (MSD $\sim \tau^x; x < 1$) extending to longer time scales for higher pressures.
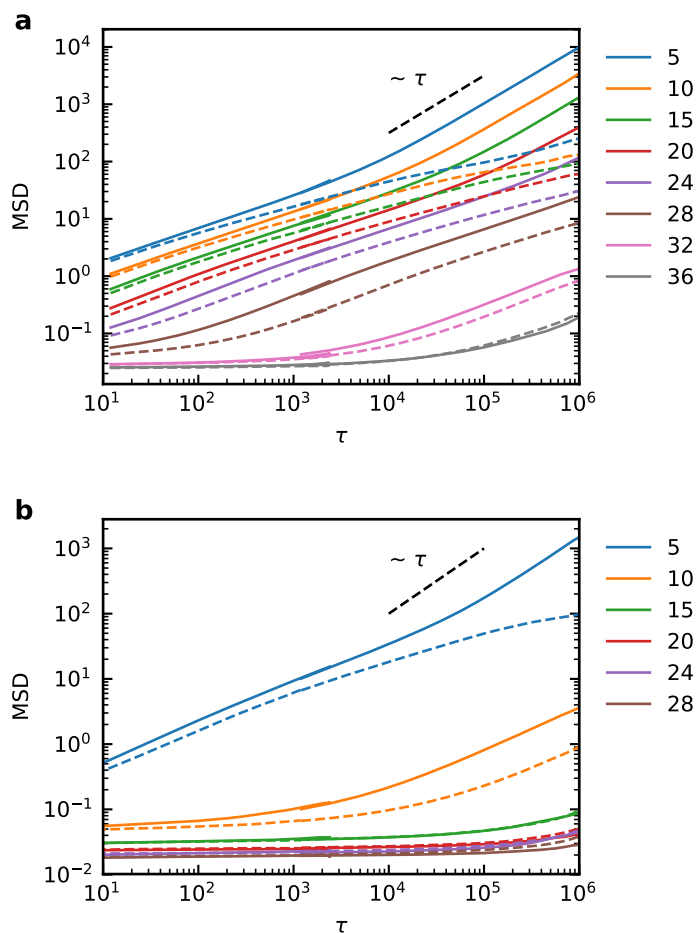

Fig. 3 Mean-squared displacements of polymer segments in neat systems (solid) and nanocomposite systems (dashed) for flexible (**a**) and rigid (**b**) systems. Legend indicates reduced pressure (P*) of each system.

However, there is still some slow relaxation occurring even at P* = 36, with segment MSDs beginning to increase at the longest time scales probed ($\tau \sim 10^5 - 10^6$). For the rigid model we see that systems with P* $\geq$ 15 have a segment MSD that remains constant even at longer time scales ($\tau \sim 10^5$) and show little relaxation even at $10^5\tau - 10^6\tau$.

The non-Gaussian parameters ($\alpha(\tau) = \frac{3}{5} \frac{\langle \Delta r^4 \rangle}{\langle \Delta r^2 \rangle^2} - 1$) of the polymer segments indicate that the crossover from sub-diffusive to diffusive motion is pushed to longer time scales as P* is increased (Figure 4), indicated by the peak in α.[44] The degree of non-Gaussian motion, or sub-diffusive motion—indicated by the magnitude of the peak—also increases as P* is increased. For P* $\geq$ 15 for the rigid model (Figure 4b) the peak of α has not yet been reached in the time scale of the simulations.

3.2 Diffusion coefficients

We calculated the diffusion coefficient of the gas particles by using their mean-squared displacements (Equation 8) in the diffusive regime. As P* increases, D, as expected, decreases as well
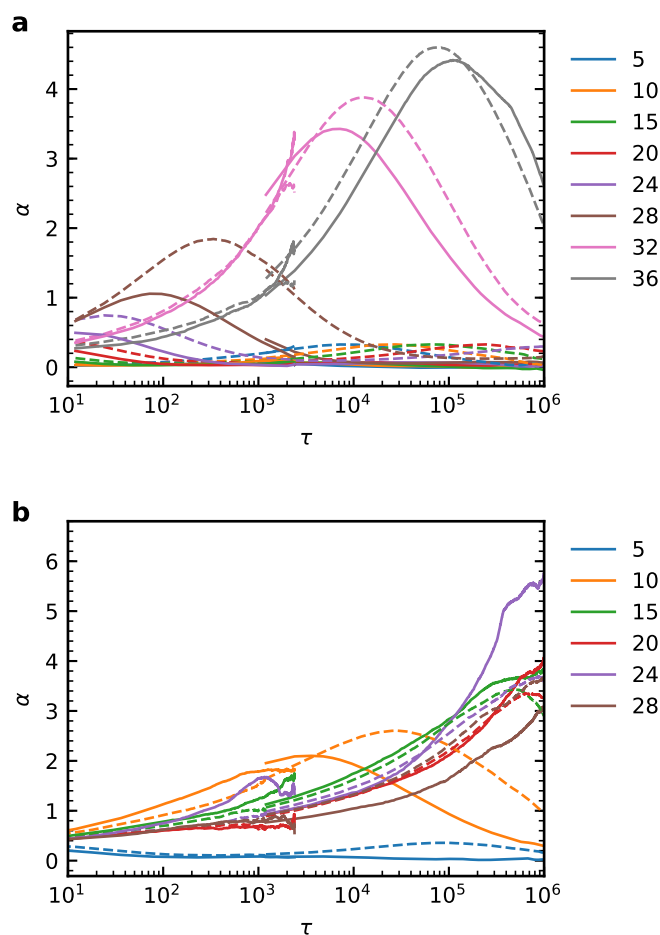
Fig. 4 Non-Gaussian parameter ($\alpha(\tau) = \frac{3}{5}\frac{\langle \Delta r^4 \rangle}{\langle \Delta r^2 \rangle^2} - 1$) of polymer segments for flexible systems (**a**) and rigid systems (**b**). Legends indicate reduced pressure, P*.

Fig. 5 Diffusion coefficients for systems with chain length 40 at the reduced pressures (P*) simulated (**a**) and diffusion coefficients of the nanocomposite systems with chain length 40 relative to the neat systems as a function of P* (**b**), for both the flexible and rigid models. Filled symbols indicate those systems which meet the minimum density for activated diffusion.[33]

(Figure 5a) in both the flexible (model I) and rigid (model II) models. The diffusivity of the gas penetrants within the rigid angle systems is also less than that of systems which use the flexible model by several orders of magnitude. This is can be explained, in part, to the slower segmental motion of the chains in the rigid systems compared to the flexible systems (Figure 3).[27]

While gas diffusion in the rigid systems is suppressed relative to that in the flexible systems, we are interested in how chain rigidity affects D when going from neat to composite systems. Systems without the added angle potential—the flexible model—require P* ≥ 24 in order to meet the minimum density needed to exhibit activated gas diffusion (filled points in Figure 5b).

For flexible systems which meet the minimum density required for activated diffusion, D is suppressed when going from the neat system to the composite system. In fact, D in the flexible composite systems is suppressed to about 40% of its value in the flexible neat systems, which is inconsistent with the Maxwell model. For all systems studied, the volume fraction of the nanoparticles is around 5 to 6% and the Maxwell model predicts that the D in the composite should be between 96 and 97% of that in the neat.
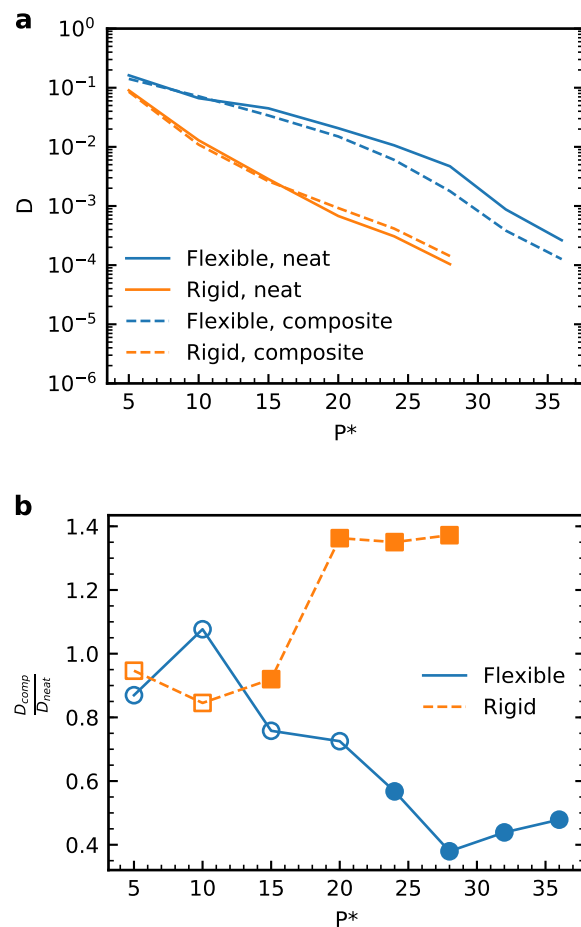
In contrast, D is enhanced in the rigid angle systems when comparing the nanocomposite systems to the neat ones for P* ≥ 20. Although P* = 15 meets the minimum density requirement for activated diffusion for the rigid model, it does not exhibit the same enhancement of diffusivity. We can conjecture, that even though the gas diffusion is activated in this system, there is a competing effect of the presence of the nanoparticles which block the gas penetrants. The diffusion suppression ($D_{comp}/D_{neat} = 0.92$) is consistent with the Maxwell prediction (0.97).

Although there is a slight diffusion enhancement for Model II for P* ≥ 20, it is much smaller than in the experiments where diffusion enhancements of 8-13 are observed (Figure 1). One possible explanation is the systems we simulated are on the "edges" of the volcano, and we need to vary the chain length in order to get to the volcano's "peak". The experimental gas permeability enhancement peak is seen when the brush height of the chains is on the order of the radius of the nanoparticle. However, the brush height for the N=40 systems is approximately 1.4 times that of

the nanoparticle radius, which means we are already close to the peak in the volcano plot.

Nevertheless, we varied the length of the graft chains at P* = 20 in order to investigate the graft length-dependence of D. When we vary the chain length for the grafted chains at P* = 20, we observe the same values of gas diffusion enhancement as the system with 40 segments per chain (Figure S8[†]). In other words, diffusion in the nanocomposites is enhanced only to about 1.3 times of that in the neat melt, no matter the chain length. Thus, our model does not capture the graft length-dependence of D seen in previous experiments (Figure 1). It also does not capture the magnitude of the experimental enhancement.

One possible explanation is that our model does not have enough chemical detail in order to capture the non-monotonic graft length-dependence of D. Recent work using broadband dielectric spectroscopy of PMA-grafted silica nanoparticles has shown that there is a small monotonic decrease in segmental relaxation time as the length of graft chains is increased.[45] However, the secondary relaxations of the PMA grafts follow the non-monotonic trend of the previously reported experimental enhancement in gas diffusion. These secondary relaxations are fastest at the peak of the volcano plot in Figure 1, showing a clear correlation between the two quantities.

Our model does not have side groups, and the secondary relaxations in the experiment are assigned to the rotations of the carboxymethyl groups in PMA. Thus, it may be necessary to model side groups in order to accurately capture the gas diffusion enhancement of the experimental PMA-grafted nanoparticles. We also note that the enhancement of D we observe in our simulations is only for glassy systems, but PMA is rubbery at the conditions of the experiment where gas diffusion was enhanced. Interestingly, that same study showed that the density at the peak of the volcano plot is also at a minimum, and we now turn our attention to discuss the polymer phase densities in our simulations to examine if this could explain the disagreement between our simulations and the experiments in Figure 1.

3.3 Polymer phase segmental densities

Previous experimental work has shown that segmental density plays an important role in gas diffusion and that lower segmental densities may be correlated with higher gas diffusivities. Thus, we investigate the polymer-phase density (ρ) of each system simulated. The density of the polymer segments in the polymer phase of each system increases as P* increases (Figure 6a). This is expected and desired since we used increasing P* to simulate above the minimum ρ in order to be in the correct parameter space that results in activated gas diffusion. Even though ρ of each system increases with increasing P*, the ρ of composites is lower than that of their respective neat systems for both the flexible and rigid models. In other words, the addition of nanoparticles and the process of grafting the free chains to them decreases ρ in all systems.

For the flexible systems the density in the composite polymer phase is 1.5% to 2.0% lower than than the neat polymer-phase density (Figure 6b). Although these systems do experience a

slight decrease in polymer phase segmental density when going from neat to composite, it is presumably not enough to overcome the effect of tortuosity and enhance diffusion in the composite. As stated above, the diffusion coefficient actually decreases in the composite flexible systems compared to the neat flexible systems, even beyond what the Maxwell model predicts.
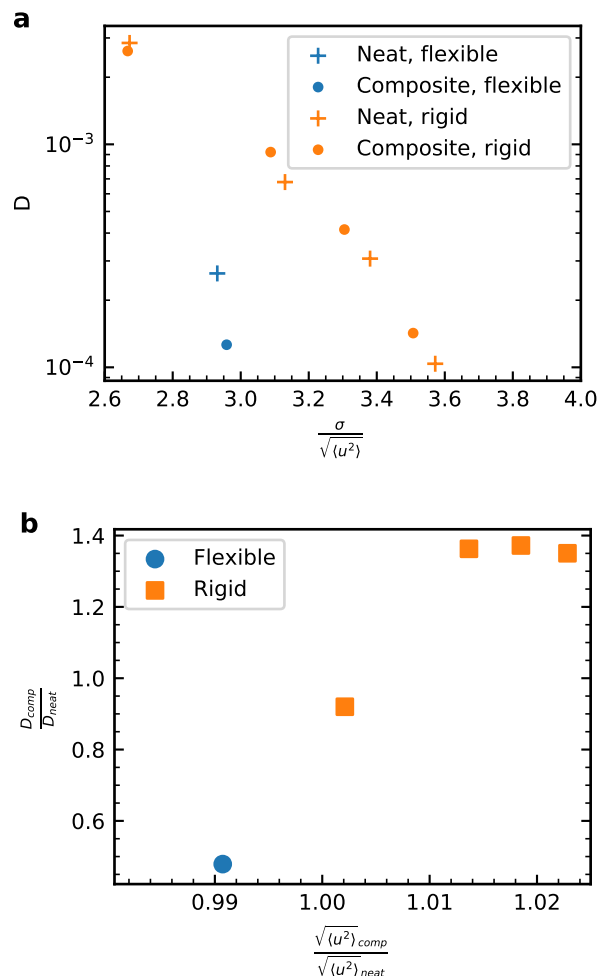
Fig. 7 a The ratio of the size of the diameter of the gas particle, 0.5σ, to the magnitude of the segmental motion, as determined by the plateau of the mean-squared displacement of the segments ($\langle u^2 \rangle$, see Figure 3) as a function of the gas particle's diffusion coefficient. Thus, larger values on the x-axis indicate smaller cage sizes for the gas penetrants. The plateau value is only available systems in the vicinity of the glass transition, which is systems with P* = 36 for the flexible model and P* ≥ 15 for the rigid model, which are shown from left to right in the figure. **b** The relative diffusivity (D_{comp}/D_{neat}) plotted against the relative cage size ($\sqrt{\langle u^2 \rangle}_{comp}/\sqrt{\langle u^2 \rangle}_{neat}$). System P*, from left to right: flexible – 36; rigid – 15, 20 ,24, 28

The rigid systems' polymer-phase density also decreases for the activated diffusion simulations of the composite systems. At P* = 5, which does not exhibit activated diffusion for the rigid model, there is little difference in the polymer-phase density when compared to the flexible model. At P* = 10 the density is already 2.5% lower than that of the neat system. For systems with P* >

10, the polymer-phase density for the rigid systems remains relatively constant. All four of those systems are about 3.3% lower in density in the composite systems compared to the neat systems. In comparison, experimental observations show a negligible decrease at the edges of the volcano plot in Figure 1 and show about a 2% decrease at the peak of the volcano where diffusion is enhanced the most.[45] Thus, the lowering of the polymer phase density in our simulations coincides with the enhancement of diffusion of the gas penetrants, but it over-represents the decrease in density when compared to experiments.

3.4 Fractional free volumes and partial molar volumes

The fractional free volumes (FFV) of the polymer phase—calculated using Equation 12—show a similar trend. Higher reduced pressures give lower polymer-phase FFV's (Figure 6c). The FFV of flexible composite systems decreases relative to flexible neat systems (Figure 6d). Conversely, rigid composite systems show a relative increase in the FFV at higher reduced pressures, with relative FFV's slightly above 1.03 for P* > 10. In addition to comparing FFV's, we calculated the "partial" molar volume (PMV) of adding a single nanoparticle to the neat system and grafting chains to it (Equation 9). The volume of a single nanoparticle calculated using Equation 11 is approximately $73\sigma^3$. For the flexible systems the PMV is approximately between 80 and $83\sigma^3$ (Figure S7a[†]). Thus the change in volume (V) of the system when going from the flexible neat system to the flexible composite system is largely dominated by the addition of the nanoparticles.

The rigid model, however, shows a much larger increase in the system volume when going from neat to composite. For P* = 5, the PMV is nearly the same as the flexible model, but at P* = 10 there is already a PMV of approximately $93\sigma^3$. The PMV of the activated diffusion systems (P* ≥ 15) remains relatively constant between 100 and $102\sigma^3$. Thus, going from the system of free chains to a system of polymer-grafted nanoparticles results in the change of V equal to 1.4 times that of a nanoparticle per grafted nanoparticle ($101\sigma^3/73\sigma^3 = 1.4$) for systems using the rigid angle model. In other words, the difference in volume of the composite and neat systems includes both the volume of the nanoparticles as well as additional "free" volume. Systems with more free volume generally show an increase in diffusivity. P* = 15 for the rigid model is the exception which we discuss below.

3.5 Cage sizes

The one outlier here in this discussion thus far is P* = 15 in the rigid model. It meets the ρ_c requirement for activated gas diffusion, and it has a polymer-phase density similar to systems with P* ≥ 20 which all exhibit gas penetrant diffusion enhancement. However, gas diffusion is not enhanced in this system and the diffusion suppression is consistent with the Maxwell model.

One metric that possibly explains this outlier is the cage size experienced by the gas penetrants.[27,46] The square root of the plateau of the mean-squared displacement of polymer segments ($\sqrt{\langle u^2 \rangle}$) is a method for calculating the cage size for a gas penetrant. This plateau value is only available for systems that are beyond the glass transition, which in this case are P* ≥ 15 for the

rigid model and only P* = 36 for the flexible model. Figure 7a shows the diffusion coefficient of the gas penetrant as a function of the gas particle's size divided by $\sqrt{\langle u^2 \rangle}$. Only two points are available for the flexible model—one for the composite system at P* = 36, and the other for the neat system at the same P*. Notably the composite system's $\sqrt{\langle u^2 \rangle}$ is slightly smaller than that of the neat system.

All of the rigid model's points seem to fall on a single curve, indicating that as $\sqrt{\langle u^2 \rangle}$ gets smaller, D of the gas increases. Specifically, diffusion is enhanced in the nanocomposite systems when $\sqrt{\langle u^2 \rangle}$ is larger than its corresponding neat system. We note that $\sqrt{\langle u^2 \rangle}$ for P* = 15 for the rigid model—in the upper left of Figure 7a is approximately the same for the neat and composite systems.

This can be more clearly seen in Figure 7b where the relative diffusivity (D_{comp}/D_{neat}) and relative cage sizes ($\sqrt{\langle u^2 \rangle}_{comp}/\sqrt{\langle u^2 \rangle}_{neat}$) are plotted. The cage size of the flexible composite system ($\sqrt{\langle u^2 \rangle}_{comp}$) at P* = 36 is smaller than the cage size of the neat system ($\sqrt{\langle u^2 \rangle}_{neat}$) at the same P*. Then looking at P* = 15 for the rigid model, $\sqrt{\langle u^2 \rangle}_{comp}$ is only slightly larger than $\sqrt{\langle u^2 \rangle}_{neat}$, and is not larger enough to overcome the tortuosity effect of the nanoparticles. In contrast, systems with P* ≥ 20 are all enhanced (upper right of Figure 7b) and have $\sqrt{\langle u^2 \rangle}_{comp}$ around 1% to 2% times larger than $\sqrt{\langle u^2 \rangle}_{neat}$. Meng et. al.[27] showed that the ratio of the size of the gas penetrant to the cage size is linearly related to the diffusivity. In agreement with that, we have shown that the size of the cage may be a more relevant descriptor of the diffusion of the gas than the polymer phase density, at least in the rigid model, since the polymer phase density is the same for the system with P* = 15 (which shows diffusion suppression) as those with P* ≥ 20 (which show diffusion enhancement).

4 Conclusion

We have shown that the diffusion of gas penetrants is enhanced in coarse-grained simulations of polymer-grafted nanoparticles when compared to their neat analogues. This enhancement only occurs in glassy systems using a rigid angle potential and at a high enough density. Additionally we did not observe any diffusivity dependence on the graft length. This conflicts with previous experimental observations of both glassy and rubbery polymer (PMA and PMMA) grafted nanoparticles. This discrepancy is potentially due to side groups not being present in our coarse-grained models. Although there is an inverse correlation between the polymer-phase density and penetrant diffusivity in our simulations—in agreement with previously reported experiments—the one quantity that most fully describes the diffusion enhancement in our simulations is the size of the cage experienced by the gas penetrant.

5 Conflicts of interest

There are no conflicts to declare.

6 Acknowledgments

References

1 R. W. Baker, *Membrane Technology and Applications*, Wiley and Sons, West Sussex, UK, 2012.

2 C. A. Scholes, G. W. Stevens and S. E. Kentish, *Fuel*, 2012, **96**, 15 – 28.

3 D. F. Sanders, Z. P. Smith, R. Guo, L. M. Robeson, J. E. Mc-Grath, D. R. Paul and B. D. Freeman, *Polymer*, 2013, **54**, 4729 – 4761.

4 H. Lin and B. D. Freeman, *Journal of Molecular Structure*, 2005, **739**, 57 – 74.

5 C. E. Powell and G. G. Qiao, *Journal of Membrane Science*, 2006, **279**, 1 – 49.

6 A. Brunetti, F. Scura, G. Barbieri and E. Drioli, *Journal of Membrane Science*, 2010, **359**, 115 – 125.

7 D. Y. Leung, G. Caramanna and M. M. Maroto-Valer, *Renewable and Sustainable Energy Reviews*, 2014, **39**, 426 – 443.

8 J. Wijmans and R. Baker, *Journal of Membrane Science*, 1995, **107**, 1 – 21.

9 L. M. Robeson, *Journal of Membrane Science*, 1991, **62**, 165 – 185.

10 L. M. Robeson, *Journal of Membrane Science*, 2008, **320**, 390 – 400.

11 B. D. Freeman, *Macromolecules*, 1999, **32**, 375–380.

12 W. Koros and G. Fleming, *Journal of Membrane Science*, 1993, **83**, 1–80.

13 W. Koros and R. Mahajan, *Journal of Membrane Science*, 2000, **175**, 181–196.

14 P. Pandey and R. Chauhan, *Progress in Polymer Science*, 2001, **26**, 853–893.

15 R. Baker, *Industrial & Engineering Chemistry Research*, 2002, **41**, 1393–1411.

16 P. Bernardo, E. Drioli and G. Golemme, *Industrial & Engineering Chemistry Research*, 2009, **48**, 4638–4663.

17 D. DÁlessandro, B. Smit and J. Long, *Angewandte Chemie International Edition*, 2010, **49**, 6058–6082.

18 H. B. Park, J. Kamcev, L. M. Robeson, M. Elimelech and B. D. Freeman, *Science*, 2017, **356**, year.

19 D. Maillard, S. K. Kumar, B. Fragneaud, J. W. Kysar, A. Rungta, B. C. Benicewicz, H. Deng, L. C. Brinson and J. F. Douglas, *Nano Letters*, 2012, **12**, 3909–3914.

20 P. Rittigstein, *Journal of Polymer Science Part B: Polymer Physics*, 2006, **44**, 2935–2943.

21 R. K. Bharadwaj, *Macromolecules*, 2001, **34**, 9189–9192.

22 J. Maxwell, 1873.

23 R. Bouma, A. Checchetti, G. Chidichimo and E. Drioli, *Journal of Membrane Science*, 1997, **128**, 141 – 149.

24 C. R. Bilchak, E. Buenning, M. Asai, K. Zhang, C. J. Durning, S. K. Kumar, Y. Huang, B. C. Benicewicz, D. W. Gidley, S. Cheng, A. P. Sokolov, M. Minelli and F. Doghieri, *Macromolecules*, 2017, **50**, 7111–7120.

25 W. M. Lee, *Polymer Engineering & Science*, 1980, **20**, 65–69.

26 Y. Huang, X. Wang and D. Paul, *Journal of Membrane Science*, 2006, **277**, 219 – 229.

27 D. Meng, K. Zhang and S. K. Kumar, *Soft Matter*, 2018, **14**, 4226–4230.

28 T. Merkel, V. Bondar, K. Nagai and B. Freeman, *Journal of Polymer Science Part B-Polymer Physics*, 2000, **38**, 273–296.

29 T. C. Merkel, B. D. Freeman, R. J. Spontak, Z. He, I. Pinnau, P. Meakin and A. J. Hill, *Science*, 2002, **296**, 519–522.

30 S. Takahashi and D. Paul, *Polymer*, 2006, **47**, 7519 – 7534.

31 N. J. Fernandes, H. Koerner, E. P. Giannelis and R. A. Vaia, *MRS Communications*, 2013, **3**, 13âĂŞ29.

32 H. Lin and B. Freeman, *Springer handbook for materials measurement methods*, Springer, Berlin, 2011, pp. 426–444.

33 K. Zhang, D. Meng, F. Muller-Plathe and S. K. Kumar, *Soft Matter*, 2018, **14**, 440–447.

34 V. Pryamitsyn, B. Hanson and V. Ganesan, *Macromolecules*, 2011, **44**, 9839–9851.

35 S. Plimpton, *Journal of Computational Physics*, 1995, **117**, 1 – 19.

36 M. Parrinello and A. Rahman, *Journal of Applied Physics*, 1981, **52**, 7182–7190.

37 G. J. Martyna, D. J. Tobias and M. L. Klein, *The Journal of Chemical Physics*, 1994, **101**, 4177–4189.

38 W. Shinoda, M. Shiga and M. Mikami, *Phys. Rev. B*, 2004, **69**, 134103.

39 M. E. Tuckerman, J. Alejandre, R. López-Rendón, A. L. Jochim and G. J. Martyna, *Journal of Physics A: Mathematical and General*, 2006, **39**, 5629.

40 K. Kremer and G. S. Grest, *The Journal of Chemical Physics*, 1990, **92**, 5057–5086.

41 R. S. Hoy, *Phys. Rev. Lett.*, 2017, **118**, 068002.

42 R. Auhl, R. Everaers, G. S. Grest, K. Kremer and S. J. Plimpton, *The Journal of Chemical Physics*, 2003, **119**, 12718–12728.

43 J. Park and D. Paul, *Journal of Membrane Science*, 1997, **125**, 23 – 39.

44 B. Vorselaars, A. V. Lyulin, K. Karatasos and M. A. J. Michels, *Phys. Rev. E*, 2007, **75**, 011504.

45 B. Carroll, E. Buenning, S. Cheng, Y. Huang, B. C. Benicewicz, A. P. Sokolov and S. K. Kumar, 2018.

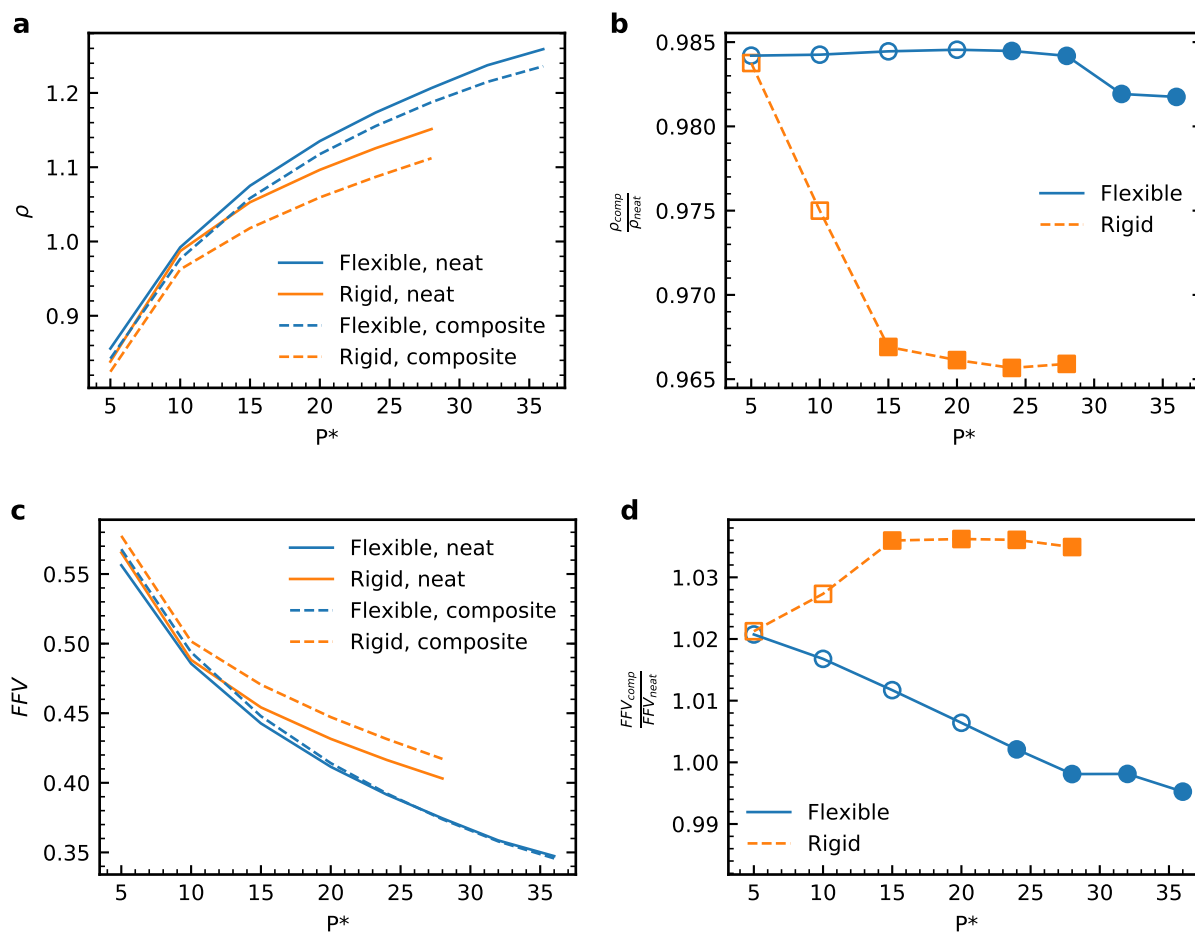46 A. A. Gusev and U. W. Suter, *The Journal of Chemical Physics*, 1993, **99**, 2228–2234.

Fig. 6 a Segmental densities of the polymer in the polymer phase for each system at the P* simulated. **b** Segmental densities of the polymer in the composite system in the polymer phrase, relative to that of the neat systems as a function of P*, for both the flexible and rigid models. Filled symbols indicate those systems which meet the minimum density for activated diffusion. **c** Fractional free volume in the polymer phase for each system at the P*'s simulated. **d** Fractional free volume of the polymer in the composite system in the polymer phrase, relative to that of the neat systems as a function of P*, for both the flexible and rigid models. Filled symbols indicate those systems which meet the minimum density for activated diffusion.